Comparing Photometric Behavior of LEO Constellations to SpaceX Starlink using a space-based optical sensor

Chance Johnson
Defence R&D Canada Ottawa, Canada
Dr. Lauchie Scott
Defence R&D Canada Ottawa, Canada
Stefan Thorsteinson
Defence R&D Canada Ottawa, Canada

ABSTRACT

To complement ground-based efforts to photometrically characterize the increasing LEO population that uses constellation-style architectures, this paper presents space-based photometric measurements of the OneWeb and Flock LEO constellations and compares them to photometric measurements of the Starlink constellation. Starlink is used as a photometric reference due to the large number of its constellation members, its simple solar panel and bus geometry, and that it is known to be bright - making space-based observing opportunities more frequent. Space-based photometric reference measurements of Starlink were collected by Canada's Near Earth Object Surveillance Satellite (NEOSSat) during a six-month observing campaign in 2020. NEOSSat characterized 247 Starlink satellites using short duration (<4 minute) optical observation tracklets totalling more than 1400 observations. It was shown that a repeatable space-based light curve of the Starlink constellation can be produced by aggregating short duration tracklets of individual constellation members. All measurements were range-normalized to 1000 km removing range-dependent variations in their photometry and to enable future comparisons with other LEO space objects. After these basic reductions, the Starlink satellites exhibit magnitudes spanning M_v ~4 – 13, with an average brightness of M_v 6.9 ± 0.9. A repeatable light curve in phase angle forming a V-shape with a minimum brightness cusp of M_v 7.5 at 90° phase angle is produced. It is shown that this V-shaped photometric behaviour is due to both a Starlink satellite's phase angle and the degree to which the Starlink reflects earthshine toward the space-based observer. In this paper, the observations of the original Starlink constellation are further complimented with an additional 675 observations of Starlinks with solar reflection minimizing visors. It is shown that from a space-based perspective there is no noticeable change in the photometry of these satellites over most phase angles. A further 1400 observations of the OneWeb satellite constellation were later collected. The OneWeb satellites exhibit magnitudes spanning M_v ~4.8 – 10.0, with an average brightness of M_v 7.4 ± 0.8, roughly half a magnitude fainter than Starlink. Finally, a small sample of photometric measurements on a nanosatellite constellation (Planet Labs Doves) were acquired and compared to the larger Starlink and OneWeb satellites. The small number of Flock measurements (28) does not enable a general comparison of their photometric behaviour to the Starlink and OneWeb satellites, but their detected, range-normalized brightness span M_v ~5.9 – 11.2 with an average brightness of M_v 9.4 ± 1.1.

1. INTRODUCTION

The proliferation of Low Earth Orbit (LEO) constellations has yielded more than 1300 satellites in 2020 and 2021 alone, accounting for roughly 40% of the entire operational satellite population [1]. The current frontrunner of these mega-constellations is SpaceX's Starlink. Shortly after its first set of satellites were launched in May 2019, Starlink raised concern within the astronomical community when ground observers decried an impact to professional survey astronomy resulting from Starlinks' bright visible signatures. In August 2020, SpaceX began equipping all Starlink satellites with a sun-reflecting visor to reduce the amount of sunlight from the Starlink satellite bus pointed toward a ground-based observer. This demonstrates Industry's willingness to collaborate with the astronomical community and assist in alleviating issues posed by the rapid growth of mega-constellations; however, debate continues as to whether enough is being done to manage the increasing risks to astronomy. In addition, Space Domain Awareness (SDA) understanding, and characterization of constellation infrastructure is still in its infancy.

This paper expands upon the preliminary findings of previous space-based observations of the SpaceX Starlink constellation. It was learned that Starlink satellites exhibit consistent nightside (low phase angle φ) and dayside (high phase angle) photometric behaviour. It was also found that by aggregating individual photometric observations on

different constellation members, a light curve can be produced by observing multiple, individual members of the constellation. This takes advantage of the mass-production style manufacturing techniques for satellites and their similar attitude profiles on orbit.

The Starlink measurements revealed relatively consistent diffuse reflection behaviour was observed on the nightside, however similarly shaped, but much more variable brightness behaviour was observed on the dayside. This effect is attributed to earthshine and the degree to which a Starlink reflects light toward the observer [2]. While earthshine's influence has been previously reported on geosynchronous satellites [3], modelling to predict LEO object brightness for a space-based observer observing a LEO over the illuminated portion of Earth was presented. Taken over all observing geometries, the Starlink constellation showed an average visual magnitude (M_v) of approximately 6.4 ± 0.8 using a 1000 km normalization range. The Starlink main solar array was estimated to have an albedo-area coefficient of 0.9 m^2 on its sun-facing side but has a more reflective backside of ~10.5 m^2. Notably, Starlink satellites incorporating reflectivity reduction treatments, such as *Darksat* and *Visorsat*, showed no noticeable difference in photometric behaviour compared to Starlink satellites unequipped with these darkening treatments [2]. In this paper, modelling and characterization of Starlink photometry is further extended, continued measurements of *Darksat* and *Visorsat* are presented, and their photometry is compared to the lower inclination members.

Other LEO constellations have been established in recent years, but with fewer members compared to Starlink; namely, OneWeb and Planet Labs Flock constellations. This paper examines how different orbit geometries influence photometric behaviour of a LEO satellite when viewed from space. These comparisons can be used to establish 'typical' characteristics of LEO constellations helping to differentiate between controlled or uncontrolled satellite attitude profiles. These comparisons can also assist in the design of future space-based optical sensors tracking space objects in-situ for collision avoidance or debris population assessment purposes. This constellation comparison can also assist the visual-survey astronomy community by providing a space-based perspective on constellation brightness helping refine observing mitigation methods or help detect faint space objects in the presence of strenuous background illumination conditions. Table 1 summarizes the constellations studied in this paper.

Table 1 – Parameters of Starlink, OneWeb, and Flock constellations

Owner / Operator	Constellation (Mission)	#Objects	#Planes	Altitude (km)	Inclination (deg)	Estimated maximum cross - sectional area* (m^2)
SpaceX	Starlink (Comms)	1646	24	550	53.8	30
WorldVu Satellites	OneWeb (Comms)	234	18	1200	87	3.6
Planet Labs	Flock (Remote sensing)	173	1	475	97.3	0.2

2. EXAMINED LEO CONSTELLATION OBJECTS

Starlink: As of May 2021, the SpaceX Starlink constellation is comprised of 1646 active satellites, by far the largest LEO constellation to date [1]. The constellation is designed to provide global internet connectivity to terrestrial users by use of bidirectional transmission in Ku and Ka band spectrum. Starlink was licensed by the U.S. Federal Communications Commission in 2018 and authorized to launch up to 12,000 satellites in total. The initial orbital configuration consists of 24 planes with 66 satellites per plane, for a total of 1,584 satellites, inclined at 53.8 degrees operating at 550 kilometers altitude [4]. The Starlink space segment (Fig. 1) utilizes a relatively unique bus geometry offering a compact launch configuration within the Falcon 9 launch fairing. Little has been published on space segment's bus or its dimensions, however it is believed to use a nadir (Earth-facing) antenna array with an articulated linear solar array pointing radially from the Earth. For the purposes of this analysis, the main solar array is estimated to be approximately 10 meters in height and 3 meters wide. The rectangular prismatic-shaped bus, based on publicly available imagery, is presumed to be approximately 3 x 1.25 x 0.1 meters in size.

OneWeb: Another growing constellation in the race to provide global satellite broadband internet is WorldVu Satellites OneWeb. As of July 2021, the OneWeb constellation is comprised of 234 active satellites [1]. This is only

a fraction of the 648 satellites planned to fly in 18 circular orbital planes inclined at 87 degrees, at an altitude of 1200 km [5]. The OneWeb Arrow satellite bus (Fig. 1) is approximately 150 kg with dimensions are approximately 1 x 1 x 1.3 meters. The span of its solar arrays is estimated to be approximately 6 m.

Flock: Planet Labs ("Planet") launched it's first set of "Dove" satellites in 2013 and now claims to operate the world's largest Earth imaging satellite fleet. When a set of Dove satellites are launched at the same time and deployed into a single orbit, they are referred to as a "Flock." According to the Planet website, their planet monitoring solution is called "PlanetScope." Since the United States Space Command Satellite catalog labels each satellite name with "Flock," this paper refers to the constellations as "Flock."

As of January 2021, the Flock constellation is comprised of 173 active satellites [1]. Fig. 1 shows a model of the "3U" CubeSat form factor (10cm x 10cm x 30cm) [6].

Fig. 1. *Left*: Starlink satellite model. *Centre:* OneWeb satellite model. *Right*: Dove satellite model. Image Credits: AGI, OneWeb, Planet Labs.

3. NEOSSAT-TO-LEO OBSERVATION APPROACH

Near Earth Object Surveillance Satellite (NEOSSat) is a 72 kg small space telescope orbiting at 785 km altitude which performs SDA research on Earth-orbiting space objects for the Canadian Department of National Defence. The spacecraft's primary payload is a 15 cm visible light Maksutov which can sense a Resident Space Objects (RSO) to M_v 16. NEOSSat was originally designed to track geosynchronous space objects but was latter adapted to track LEO objects in 2016 following attitude control system changes. Further details on NEOSSat can be found in reference [7].

When planning space-based observations of LEO objects, several constraints must be adhered to collect space-based SDA imagery.

- NEOSSat's star tracker is not obscured by the Earth during fine slews
- The target's grazing angle is greater than 10° above the Earth limb to avoid atmospheric scattered light
- Target maximum angular rate: 220 arc-sec/sec
- NEOSSat line-of-sight solar exclusion angle: 45°
- NEOSSat line-of-sight lunar exclusion angle: 5°
- Target must be in direct sunlight
- Minimum temporal access duration between NEOSSat and the target is at least 90 seconds
- NEOSSat roll selected such that instrument radiator points (preferentially) toward deep space

Additional considerations are needed when observing LEO space objects. NEOSSat acquires imagery at a rate of 1 full frame image every 15 seconds in its 2x2 instrument binning mode. Binning the instrument enables faster sampling cadence to help acquire data on LEO objects. With this strategy, NEOSSat collects images in tracks of 4 frames where NEOSSat slews to match the average angular rate of the RSO relative to NEOSSat over the slew duration (75 seconds). Since characteristic LEO object ranges are observed at ranges greater than 10 times closer than deep space objects, large LEO space objects' apparent magnitude can be very bright. This can lead to saturation of the NEOSSat imager and image times are shortened to ~0.4 seconds to compensate on larger LEO objects.

Candidate RSOs for observation are planned with Two-Line Element (TLE) data from Celestrak.com and Systems Tool Kit software by Analytical Graphics to predict RSO position in relation to NEOSSat. NEOSSat can track LEO

objects during brief windows where all spacecraft imaging constraints and slewing capabilities are met. These windows differ slightly depending on the constellation of satellites and the observing geometry relative to NEOSSat, but typically occur as a RSO is rising or setting close to the Earth limb.

Starlink: Starlink satellites orbit Earth approximately 235 km below the altitude of NEOSSat. This causes all Starlink observing windows to occur near the Earth's limb relative to NEOSSat at ranges of ~1600-3000 km, at elevation angles from NEOSSat only varying slightly from -15° to -18°. Fig. 2 shows two example Starlink satellites orbiting over the Earth's nightside and dayside portions. This strongly influences the amount of light reflected from their surfaces. When NEOSSat observes a Starlink satellite over the nightside (low phase angles), the Starlink is primarily Sun illuminated. When observing a Starlink over the dayside, the Starlink is both Earth and Sun illuminated which influences the detected photometry. In Fig. 2 the depth of terminator angle ξ parameterizes the amount of Earth reflected sunlight which can illuminate a Starlink, or other LEO satellite, in Earth orbit.

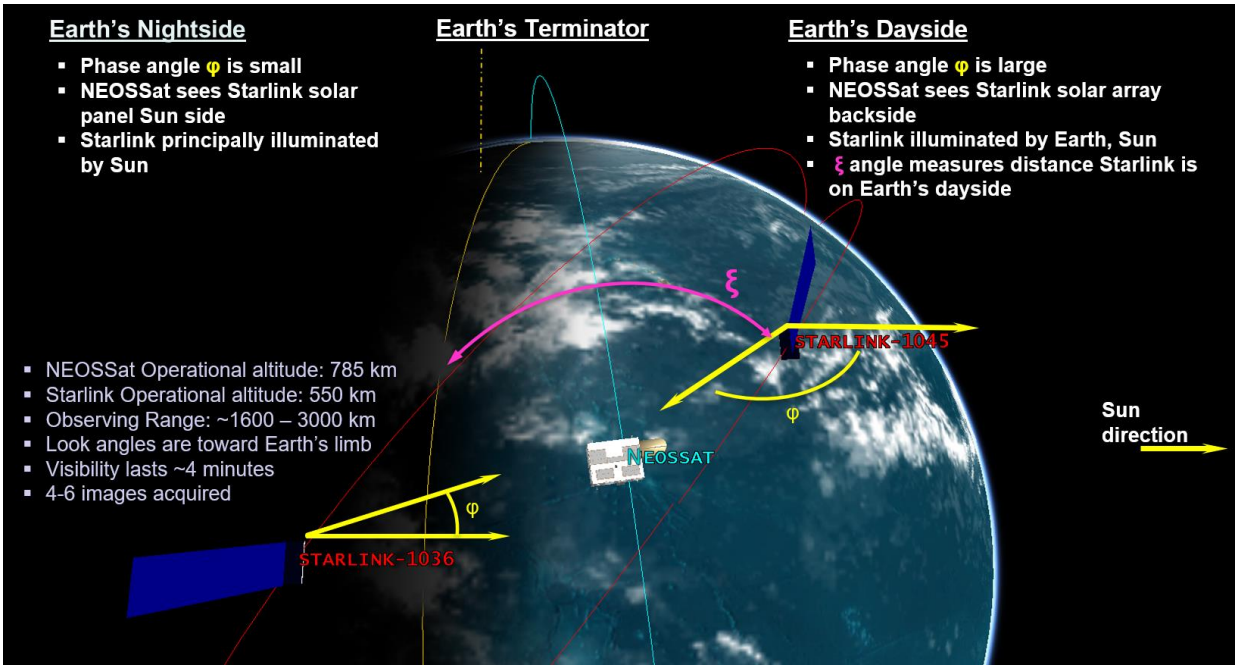

Fig. 2. Typical observing geometry of NEOSSat to Starlink showing the nightside and dayside.

OneWeb: OneWeb satellites are typically 400 km above NEOSSat's orbit altitude, resulting in varying elevations of -15° up to 30° above NEOSSat's local horizontal plane. This causes the majority of OneWeb observing windows to occur at ranges of ~2000 – 4200 km. Due to their higher altitude, OneWeb satellites have longer access durations and exposures can be longer to track fainter objects. NEOSSat instrument exposure times were set to 0.6 seconds to maximize detection and properly sample their brightness without saturation.

Flock: Dove satellites are typically 310 km below NEOSSat's orbit altitude and are somewhat more challenging to observe. Like Starlink satellites, the majority of observing windows for the Doves occurred near the Earth's limb relative to NEOSSat providing short duration observing opportunities. Typical measurement ranges spanned ~1700 – 2500 km. during NEOSSat observations on the Flock satellites. Dove satellites tended to be smaller, hence less bright compared to the larger Starlink and OneWeb satellites. Exposure times were set to 1 second to increase detectability.

4. NEOSSAT OBSERVATIONS

As NEOSSat operates without a filter a check of instrument sensitivity to varying object spectra was performed prior to satellite observation. Landolt Special Areas 97 and 108 [8] were observed and the fit of stellar color index *B*-*V* versus NEOSSat instrumental magnitudes per count is shown in Fig. 3 (left). Assuming satellite objects observed by NEOSSat reflect sunlight with spectral content similar to the Sun (*B*-*V* ~ 0.66), a zeropoint of 21.6 magnitudes/count was used in this constellation observing campaign. The estimated error of NEOSSat measurements to the actual visual

magnitude of the Landolt stars was found to be in within 0.25 magnitudes and is found by taking the residuals to the line of best fit of NEOSSat detected magnitude to the true Landolt Star visual magnitude (see Fig. 3 right). Detections reported in the following sections have an inherent uncertainty of 0.25 magnitudes due to the open-filter nature of the NEOSSat instrument.

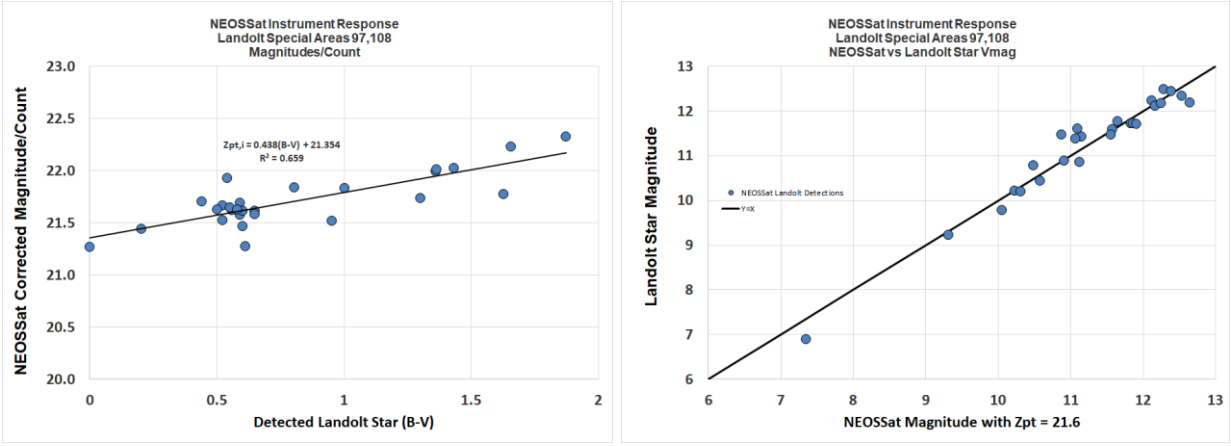

Fig. 3. *Left*: NEOSSat zeropoint as a function of stellar color index (*B-V*) for Landolt Special Areas 97, 108. *Right*: NEOSSat detected Landolt star vs actual Landolt Star visual magnitude using 21.6 as the zeropoint. The RMS residual error between NEOSSat detections vs Landolt star visual magnitudes is 0.25 magnitudes.

Starlink: NEOSSat observations of various Starlink satellites began in January 2020. Fig. 4 shows a composite of NEOSSat imagery acquired during a successful track on a single Starlink. The Starlink is identifiable as a larger, multi-pixel point source near the middle of the frame with background stars visible as short streaklets. Once imagery was downloaded, image processing consisting of registering the magnitude of the satellite along with other image metadata was performed using an astronomical imaging software program called MaxIm DL™.

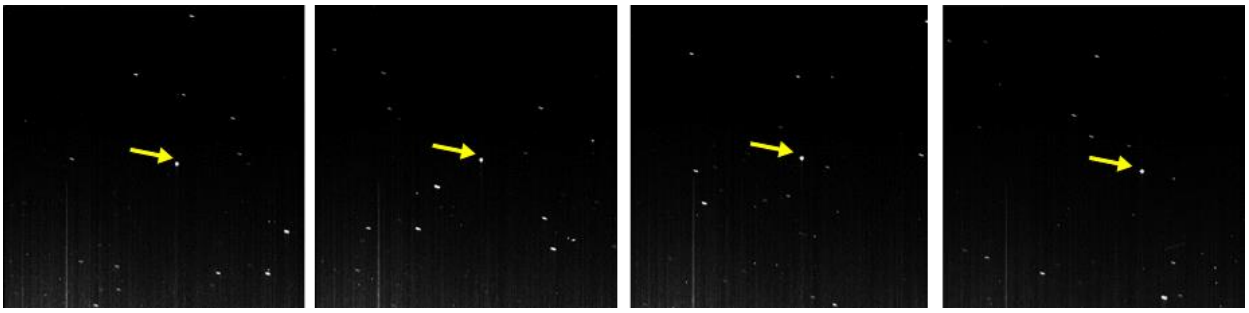

Fig. 4. NEOSSat images of STARLINK-1308, captured on 21 Jun 2020

Details on early observation attempts of the Starlink satellites are offered in the previous findings [2]. Several challenges were encountered during observation of Starlink satellites from orbit due to the relatively high orbital uncertainty invoked from Starlink's low elevation relative to NEOSSat and frequent use of electric thrusting on orbit. Approximately 30% of NEOSSat observations of Starlink satellites failed during the initial attempts at observing.

Two key factors that contributed to increasing the rate of success for observations were: 1) limiting observations to "setting" Starlink satellites, allowing NEOSSat's star tracker to observe guide stars for longer while NEOSSat observes the Starlink satellite; and 2) limiting observations to satellites in a relatively 'stable' orbit. Orbit stability was assessed by examining the Root Mean Square (RMS) orbit residuals provided by SpaceX-supplied ephemeris which were converted to TLEs by Celestrak.com [9]. It was determined that an RMS value less than 0.3 km was consistent with Starlinks which were not undergoing electric thrust orbit raising or altitude station keeping. Such TLEs were more trustworthy for tasking NEOSSat to increase the likelihood of detecting its target.

Other failed observation attempts were attributed to unique environmental effects such as the South Atlantic Anomaly (SAA) and instrument saturation while attempting to track Starlink satellites near the bright Earth limb illuminated by the Sun [2]. An example for each of these cases can be seen in Fig. 5 below.

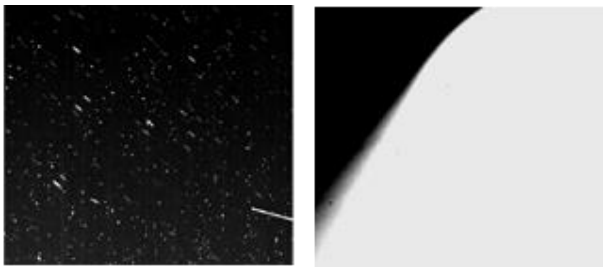

Fig. 5. NEOSSat images of unsuccessful observation attempts due to SAA (*left*) and Earth glow (*right*) [2].

OneWeb: OneWeb observations were comparatively easier to acquire due to their elevations relative to NEOSSat being up to 30 degrees above the local horizontal. At these elevations, straylight from the bright Earth limb is negligible. Fig. 6 shows a set of example frames of a OneWeb satellite observed by NEOSSat. Imaging the OneWeb constellation followed a similar approach to Starlink. As the constellation also uses constant thrust propulsion for long durations after launch, TLEs for imaging were chosen among those with lower fit RMS values from CelesTrak to ensure non-maneuvering status. OneWeb's higher altitude meant that access windows to NEOSSat were longer, often permitting multiple tracks of the same satellite during one pass, with much less interference from Earth glow.

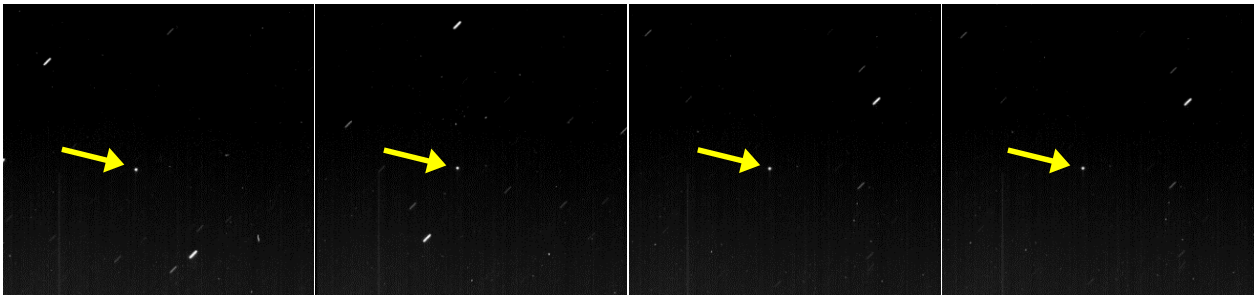

Fig. 6. NEOSSat images of ONEWEB-0025, captured on 28 June 2021

Flock: The lower altitude of Dove remote sensing satellites relative to NEOSSat tended to produce challenging observations due to stray light and the faintness of the nanosatellites observed at range. NEOSSat collected few observations on the Flock satellites during this experimentation mainly due to schedule limitations on data collection.

The Flock constellation was imaged in similar fashion to Starlink, with a slightly longer exposure time (1 s) to enhance the detectability of the smaller 3U CubeSat with its deployed solar array. Longer exposures were considered to improve throughput, but this came at the cost of additional Earth glow. Fig. 7 shows one track of imagery with a Flock just barely visible against an elevated background from Earth glow.

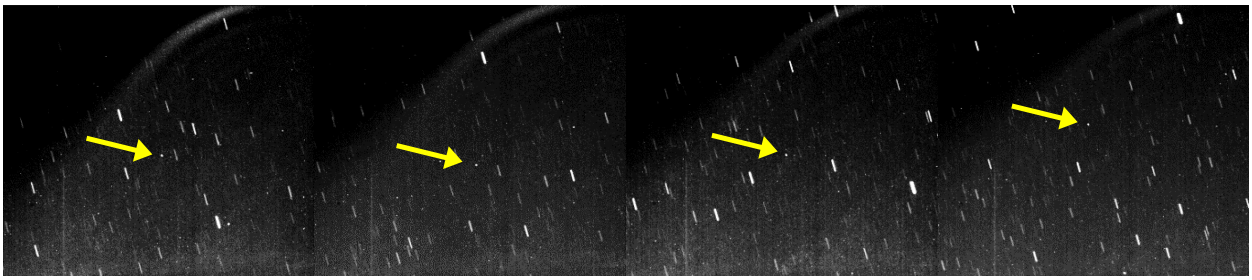

Fig. 7. NEOSSat images of FLOCK 4S-36, captured on 07 June 2021

5. STARLINK CHARACTERIZATION / RESULTS

From January 2020 to July 2021, NEOSSat acquired 2170 photometric measurements on 412 unique Starlink satellites (~25% of the constellation). NEOSSat tends to saturate its detector when target apparent magnitudes are brighter than M_v 8-8.5, with the presence of dayside sky glow exacerbating this effect. Unfortunately, a portion of this measured Starlink population did have at least 1 saturated pixel on NEOSSat's detector. Fig. 8 shows the detected magnitudes of Starlink satellites including saturated detections. Although the saturated data generally followed the photometric trend of the objects, and many unsaturated measurements are interspersed within the full set, the photometric modeling analysis omits the saturated detections. Fig. 9 shows the range normalized (R_0 = 1000 km) photometry for all data spanning 2020-2021.

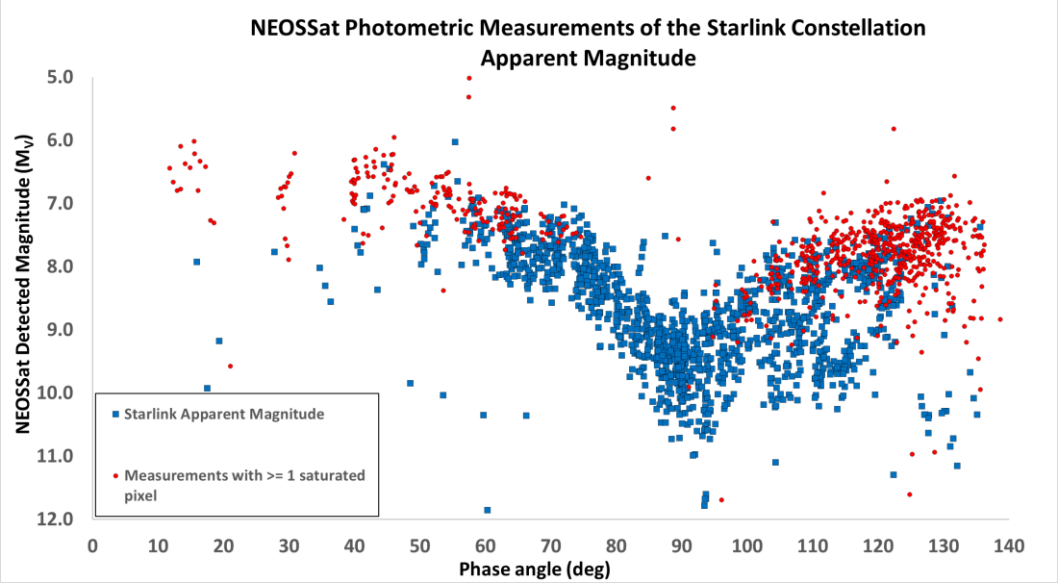

Fig. 8: Apparent magnitudes of Starlink satellites vs phase angle (saturated detections highlighted in red).

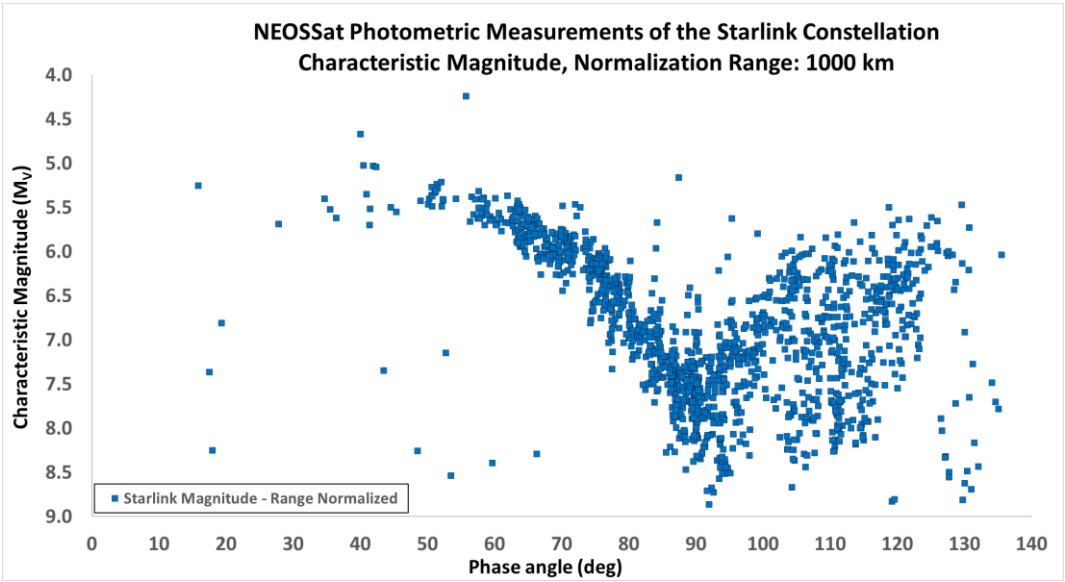

Fig. 9: Range normalized magnitudes of Starlink satellites vs phase angle.

The range normalization in Fig. 9 emphasizes two primary areas of photometric behavior unique to this constellation's "aggregated" light curve. A nightside (antisolar) and dayside photometric factor produces split behavior in the constellation's brightness divided by 90° phase angle. To analyze Starlink's brightness, the photometric data is partitioned into nightside and dayside photometry models. For phase angles (φ) less than 90° (antisolar observations), a Starlink satellite is primarily Sun-illuminated with its main solar panel aligned to the satellite position vector. The measurements in Fig. 9 tend to be consistent with about 0.5 magnitudes of variability. Above 90 degrees phase angle, the photometry is more variable (~2 magnitudes) and is influenced by both Earthshine and sunlight reflected the Starlink structure.

Nightside/Antisolar Model: Assuming that a Starlink's solar panel's power generating face is Sun-pointing, and the NEOSSat observations occur in-plane with the Starlink, a first-order photometric model of Starlink using a flat-plate solar panel facet and a short-height cylindrical bus viewed edge on is modelled as

$$M_{\varphi<90^\circ} \approx M_{Sun} - 2.5log_{10}\left(\frac{1}{\pi}\cdot\frac{a_{sp}A_{sp}\langle\cos(\varphi)\rangle}{R^2}\right) - 2.5log_{10}\left(\frac{a_{bus}A_{bus}F(\varphi)}{R^2}\right) \quad (1)$$

where the phase function for a diffusely illuminated cylinder is given by

$$F(\varphi) = \frac{1}{4\pi}\{(\pi - \varphi)\cos(\varphi) + \sin(\varphi)\} \quad (2)$$

and M_{Sun} is the magnitude of the Sun (-26.74), a_{sp} is the diffuse albedo of power generating (Sun-facing) side of the solar panel, A_{sp} is the cross-sectional area of the solar panel, φ is the target centric phase angle, R is the range to the satellite (1000 km), a_{bus} is the albedo of the cylindrical bus and A_{bus} is its cross sectional area (diameter x height) [2].

The best fit antisolar model to the measured Starlink data (with contributions from both the solar panel and the cylindrical bus overlaid) is shown in Fig. 10.

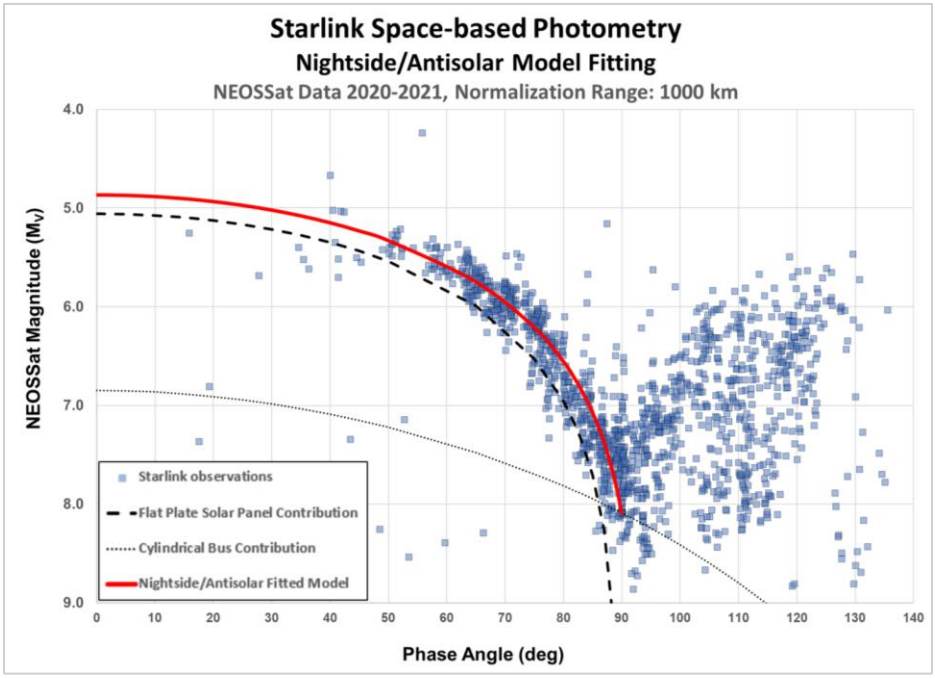

Fig. 10: Nightside/Antisolar (phase angles < 90°) photometric model for Starlink using a flat plate solar panel and short height cylindrical bus

The model uses a solar panel diffuse albedo a_{sp} of 2%, and solar panel cross-sectional area A_{sp} of 30 m^2. The estimated bus albedo a_{bus} of 0.7 and cylinder dimensions of 0.1 m radius x 1.05 m height is used. This simple model does a

reasonable job predicting the detected space-based Starlink photometric behaviour over phase angles $\varphi \sim$ 40-90° where the Sun is the primary illumination source. The good agreement of the antisolar model with the detected Starlink photometry suggests that the Starlink solar panel is largely Sun-pointing during operation. This assumption will be extended to the analysis of Starlink's dayside's photometric behaviour as it is likely that the solar panel continues its Sun pointing behaviour on either side of Earth's terminator.

Dayside Model: Dayside photometric modelling requires modelling the amount of light reflected from the Earth's surface. A linearized model is described below incorporating both Earthshine and direct sunlight on the bus and solar panel of a Starlink satellite. This hemispheric surface that a Starlink satellite "sees" on the horizon is approximated as a flat illuminated disk (see Fig. 11). To help parameterize this analysis for other constellations, non-dimensionalized parameters scaling the LEO satellite's altitude, *h*, to the Earth radius $R_\oplus$ is parameterized as $H = h/R_\oplus$. This disk of radius *c* approximates the actual surface are illuminated by the Sun.

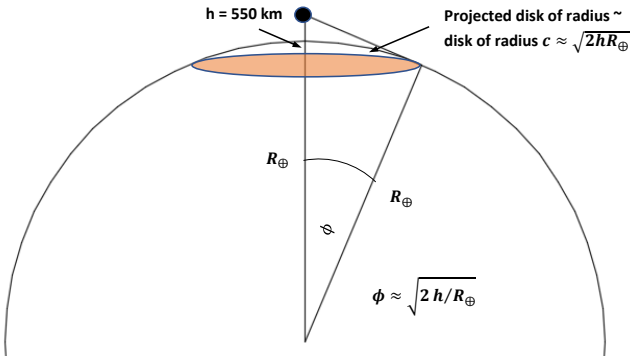

Fig. 11: Flat disk approximation of the sector of Earth "seen" by a LEO satellite [2]

Two contributions make up the total detected dayside flux reflected from a Starlink satellite and is dependent on the position of the Starlink satellite relative to the Earth's terminator (see Fig. 12). The orange patch Q_1 is the fraction of Earth reflected sunlight visible to the main solar array within the Starlink's local horizon between the subsatellite point and the terminator line. The yellow patch Q_2 is the additional portion of daylit Earth forming a near isotropic illumination pattern around the satellite bus.

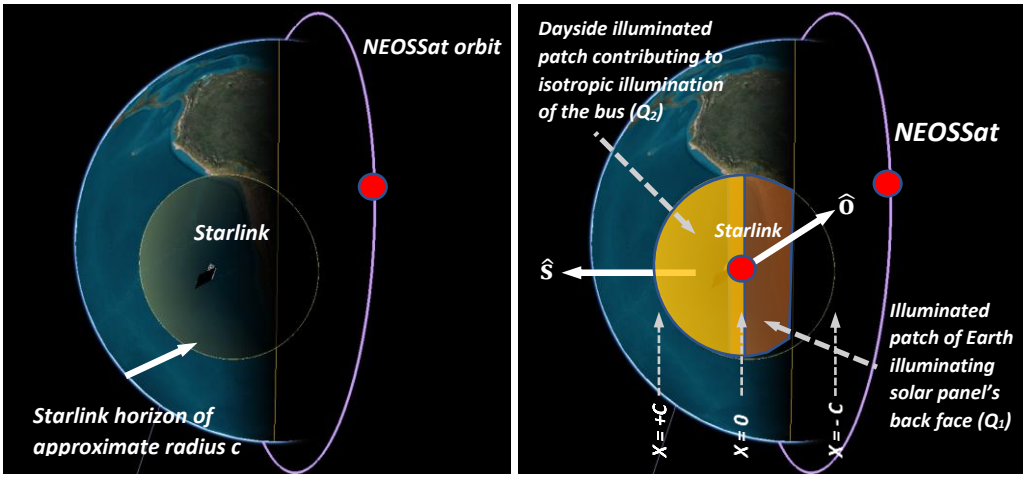

Fig. 12: *Left*: disk of earth horizon visible to Starlink satellite with illuminated patch shown. *Right*: Observer vector ô and Sun vector ŝ showing primary Earth illumination sources Q_1 and Q_2

The Starlink solar panel, modelled as a Sun-pointed flat plate, is assumed to "see" only the portion of dayside illuminated Earth relative to the terminator line. This is shown as the orange shaded region on Fig. 12 (right) and

denoted as Q_1. An estimate for the illumination this segment produces on the back of the solar panel was previously described and modelled as

$$F_{\oplus} \approx \frac{F_{Sun}}{\pi} a_{\oplus} \langle \hat{\mathbf{n}} \cdot \hat{\mathbf{s}} \rangle \left\{ 2 \int_0^{\sqrt{\frac{2}{H}}} \int_0^{\sqrt{\frac{2}{H} - X^2}} \frac{dXdY}{(1 + X^2 + Y^2)^{3/2}} \right\} \tag{3}$$

where $X = \frac{x}{h}$, $Y = \frac{y}{h}$ and $H = \frac{h}{R_{\oplus}}$ [2]. The double integral inside the curly braces is the *illumination factor* Q_1 of the Earth. After integrating equation 3 numerically (see Fig. 13), the view factor Q_1 can be approximated as $Q_1 \approx 2.54 \cdot \left(1 - e^{X/1.1}\right)$ where $X = x/h$ is the scaled linear distance from a Starlink's sub-satellite point to the Earth's terminator relative to the altitude *h* of the LEO satellite.

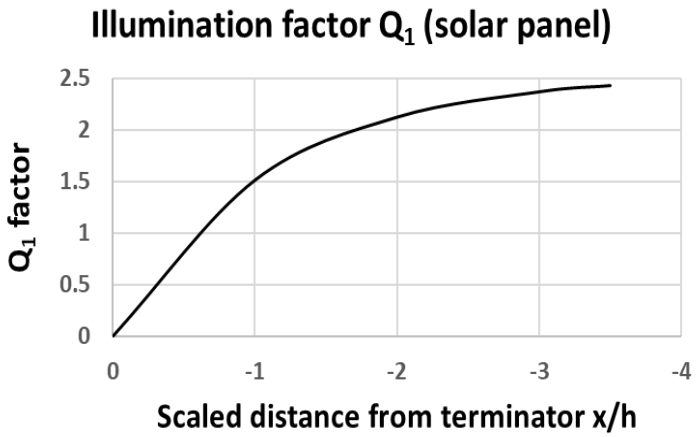

Fig. 13: View factor of illuminated fraction of Earth [2]

The satellite bus, modelled as a short height cylinder, is assumed to be isotopically illuminated when the Starlink is over the dayside of the Earth. This coarse model of the satellite bus illumination uses contributions of dayside flux from the Earth from both *Q1* and *Q2* as marked in Fig. 12 (right). Equation 3 is used to compute the total contribution for both Q_1 and Q_2 however, Q_2 uses integration limits spanning the distance from the terminator *X* to the radial limit of the illuminated portion of the disk *c* (or *2/H* non-dimensionalized). The plot Q_{total} is shown in Fig. 14 and is numerically approximated as $Q_{total} \approx 4.84/(1 + e^{1.466X})$.

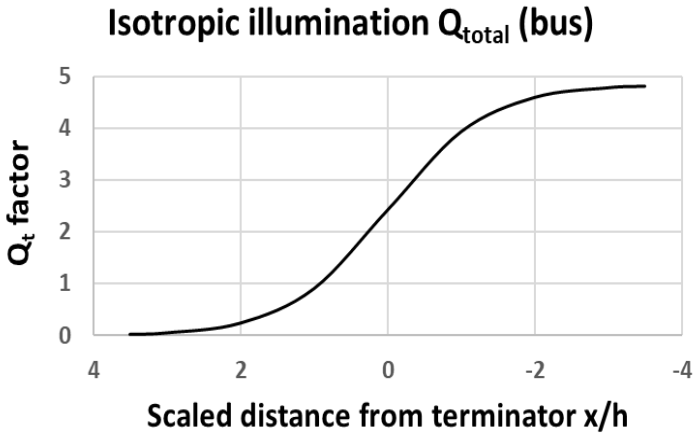

Fig. 14. Numerical integration of equation 3 to estimate the isotropic illumination factor for the Starlink satellite bus

The overall dayside model of the Starlink satellite for phase angles greater than 90°, incorporating illumination from the Earth is expressed as

$$M_{\varphi>90^\circ} = M_{Sun} - 2.5log_{10}\left(\frac{1}{\pi}\cdot a_{\oplus}\langle\hat{\mathbf{n}}_{patch}\cdot\hat{\mathbf{s}}_{patch}\rangle\right) - 2.5log_{10}(Q_1) - 2.5log_{10}\left(\frac{1}{\pi}\cdot\frac{a_{sp_{back}}A_{sp_{back}}\cos(\varphi-\pi)}{R^2}\right) - 2.5log_{10}(Q_{total}) - 2.5log_{10}\left(\frac{1}{\pi}\cdot\frac{Dha_{bus}}{R^2}\right) - 2.5log_{10}\left(\frac{1}{\pi}\cdot\frac{a_{bus}A_{bus}F_{bus}(\varphi)}{R^2}\right) \quad (4)$$

where $a_{\oplus}$ is the Earth's albedo, $\hat{\mathbf{n}}_{patch}$ and $\hat{\mathbf{s}}_{patch}$ are the Earth Centred Inertial unit vectors of the satellite position vector and Sun vector, and Q_1 is the contribution of the portion of the day-lit Earth illuminating the Starlink solar panel, $a_{sp_{back}}$ is the albedo of the space-facing side of the solar panel, $A_{sp_{back}}$ is the area of the solar panel (30 m^2), Q_{total} is the flux from both Earth illuminated regions Q_1 and Q_2, D is the diameter of the modelled cylindrical bus, h is the cylindrical bus's height and a_{bus} is its albedo. The global average value Earth's albedo $a_{\oplus} = 0.3$ [3] is used which ignores local reflectivity variations due to Earth's Ocean, land masses, polar regions, and atmosphere.

The degree to which the Starlink is over the Earth's dayside is parameterized by the angle ξ which is the *depth of terminator* of the Starlink's sub-satellite point to the terminator line.

$$\xi = 90 - \text{acos}\left(\langle\hat{\mathbf{n}}_{patch}\cdot\hat{\mathbf{s}}_{patch}\rangle\right) \approx \text{asin}\left(\frac{-x}{R_{\oplus}}\right) \approx -\frac{x}{R_{\oplus}} \quad (5)$$

where $R_{\oplus}$ is the Earth's radius. Positive values ($\xi > 0$) indicate the satellite is over the illuminated portion of the Earth where dayside flux contributions need to be considered.

Fig. 15 reveals that the isotropic contribution from the dayside illuminated cylindrical bus is very small in comparison to the to the light reflected from the Starlink solar panel and sunlight diffusely reflected from the cylindrical bus at high phase angles. For modelling, the isotropic contribution from the bus can be safely neglected at high phase angles in favour of the contributions from the Starlink solar panel and diffuse reflection from the Starlink bus. Fig. 16 shows the same data with envelopes for the total dayside fitted model for various depths of terminator angle ξ.

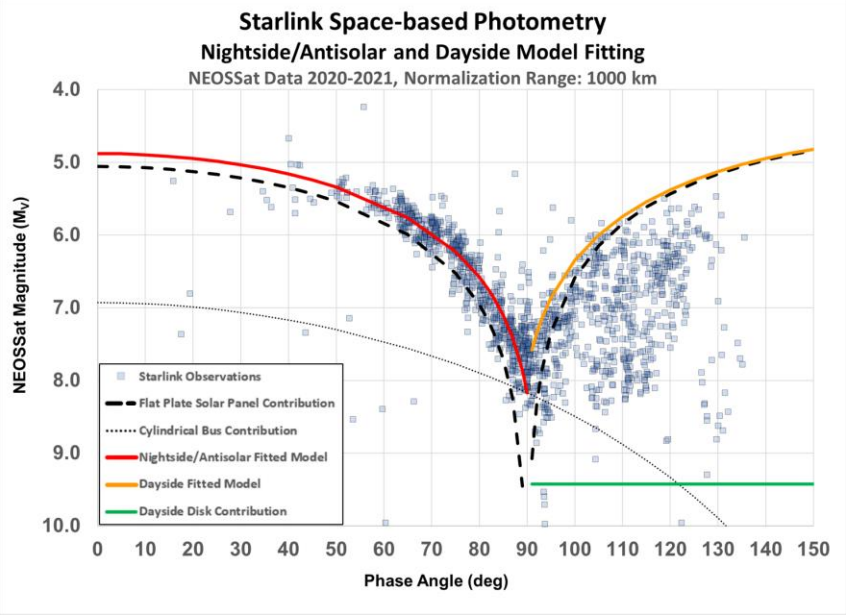

Fig. 15: Nightside/Antisolar (phase angles < 90°) and dayside (phase angles > 90°) modelling of Starlink photometry for bus and solar panel contributions to the dayside light curve

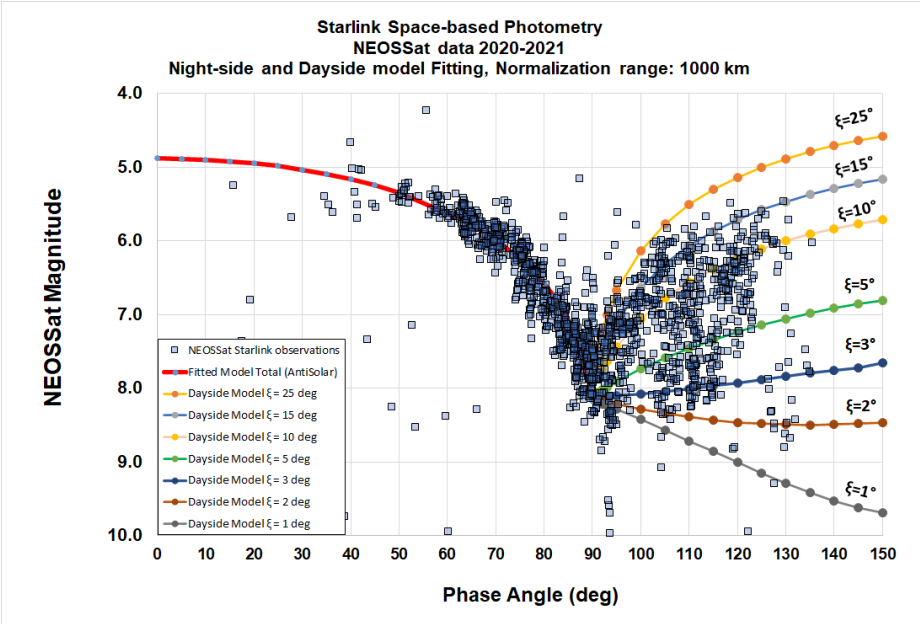

Fig. 16: Nightside and dayside modelling of Starlink photometry for various dayside depths of terminator

The modelling suggests that the main contributor to the increasing brightness, with phase angle over Earth's dayside is primarily due to the Starlink solar panel's backside [2]. The depth of terminator ξ creates illumination envelopes encompassing the variable brightness of Starlink satellites when NEOSSat when over the Earth's dayside. The albedo of the Starlink solar panel's space-facing side that best fits these ξ envelopes (Fig. 16) is estimated to be 0.35.

The Starlink solar panel is the largest contributor to the detected dayside photometry with an albedo-area product of ~10.5 m^2 assuming a 30 m^2 panel cross-sectional area. In contrast, the Sun-facing side of the Starlink solar panel has a more modest albedo-area product of ~0.9 m^2. The bus, modelled as a short height cylinder with an estimated diameter of ~2.1 m and 0.1 m height appear to have an albedo-area product of approximately 0.14 m^2. The addition of 675 new observations of Starlink in 2021 did not significantly change the albedo-area estimates in comparison to the previously reported results in [2]. The addition of a basic dayside illumination model for the Starlink bus also had a negligible impact on the results of analysis. When observed from space, the majority of reflected sunlight detected from an active Starlink satellite comes from its solar panel. This contrasts with the experiences of ground-based observers who observe the reflective nadir underside portion of the Starlink bus.

Table 2 – Key photometric findings from space-based measurements of the Starlink satellite

Starlink Facet	Assumed Geometry	Direction	Albedo-Area product (m2)	Notes
Solar Panel	Flat plate, 3 m wide x 10 m height	Sun-facing side Space-facing side	0.9 10.5	Nightside model Dayside model
Bus	Cylinder, 2.1 x 0.1 m height	Bus edge	0.14	Nightside/ Dayside model

NEOSSat measurements show few measurements below 20° phase angle thus specular reflections from the Starlink solar panel are typically not observed. This is due to the high relative angular rates of a Starlink satellite with respect to NEOSSat under that viewing geometry. NEOSSat's attitude control system is unable to maintain tracking when

angular rates exceed 220 arcseconds/sec. As such, few measurements are available within the specular reflection direction of Starlink solar panels. However, some low phase angle saturated measurements are shown in Fig. 8 and are possibly due to specular reflection from the solar arrays.

***Darksat* and *Visorsat*:** NEOSSat measurements included 25 observations of Starlink-1130 (also known as *Darksat*) and 514 observations of Starlinks equipped with a sun-reflecting visor (*Visorsats*). Measurements on these objects, shown in Fig. 17, largely followed the lopsided *V*-shaped trend with some lower magnitudes detected moving outwards in both directions from 90° phase angle.

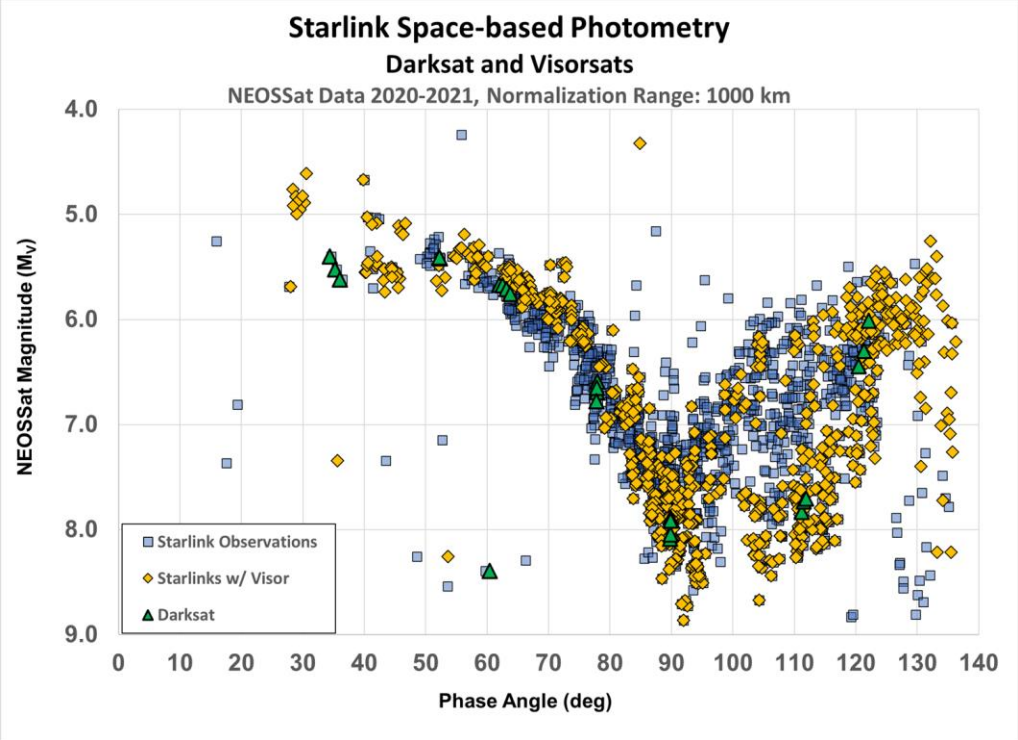

Fig. 17: Range normalized photometry of Starlink-1130 (*Darksat*) and Starlinks equipped with a sun-reflecting visor (*Visorsats*) vs phase angle

Measurements of *Darksat* typically followed the overall trend for detected magnitude versus phase angle and the average magnitude was virtually no different than the overall Starlink measurements (within 0.13 magnitudes), but with a slightly higher standard deviation of 1.35 magnitudes. The small sample size for these measurements (after eliminating saturated measurements) was not complete enough for photometric comparison with the other Starlinks.

The average brightness for Starlink satellites equipped with a sun-shading visor (also known as *Visorsats*) was virtually the same as the overall average Starlink brightness (within 0.26 magnitudes). Overall, it was found that the photometric behaviour for *Darksat* and *Visorsats* appears consistent with all other Starlink satellites when observed from a space-based vantage point. This was anticipated as reflectivity treatment changes on both *Darksat* and *Visorsats* are suggested to affect the nadir-facing portions of their buses. As NEOSSat observes the constellation from above, it primarily observes the Starlink solar array which is unaffected by changes in reflectivity on the nadir face of the bus.

6. STARLINK COMPARISON TO GROUND-BASED MEASUREMENTS

Starlink satellites have been observed from the ground with magnitudes ranging from 3.2 to 7.5 [10]. Anthony Mallama, an astronomer at the University of Maryland composed 830 Starlink observations from multiple different sources and determined an average M_v of 5.93 ± 0.02 [11]. The range normalized photometry of the Starlink constellation measured by NEOSSat, not including saturated measurements, varied from as bright as M_v 4.0 to as dim as M_v 13.0, and resulted in an average M_v of 6.9 ± 0.9. This is almost a full magnitude lower than current ground

measurements and is mainly attributed to the large number of satellites observed at lower relative phase angles with lower overall detected magnitudes.

In addition, Mallama composed more than 600 measurements of *Visorsats* and determined an average M_v of 7.18 ± 0.03 [12]. The range normalized photometry of *Visorsats* measured by NEOSSat, not including saturated measurements, varied from as bright as M_v 4.6 to as dim as M_v 13.0, and resulted in an average M_v of 6.8 ± 1.1. When observed from space the presence of the visor does not noticeably impact the photometry of the satellites and the observed brightness is a function of the phase angle and illumination conditions.

7. ONEWEB CHARACTERIZATION

From February to July 2021, NEOSSat acquired 1400 photometric measurements on 81 unique OneWeb satellites. The space-based range normalized photometry of the OneWeb constellation as a function of phase angle is shown in Fig. 18. The OneWeb constellation's brightness spans M_v 4.8-10.0, averaging M_v of 7.4 ± 0.8 with no self-consistent phase angle trends visible on either the nightside or dayside in the aggregated light curve. In general, the OneWeb satellite bus, when viewed from space does show a general decrease in brightness with phase angle but with more variability in the photometry compared to Starlink. The light curve also shows a possible slight increase in brightness over the dayside of the Earth for phase angles above 90 degrees, but the results are somewhat inconclusive due to the high variability in the measurements collected to date. OneWeb satellites show some evidence of a fall-off in dayside brightness at phase angles >130° but is much less pronounced than the Starlink data (see Fig. 17). OneWeb's higher altitude enabled NEOSSat to observe smaller phase angles in comparison to Starlink satellites. OneWeb's higher altitude and slower orbital velocity creates observing geometries where the relative angular rate of OneWeb is lower. This makes OneWeb easier to track with NEOSSat's attitude control system limitations.

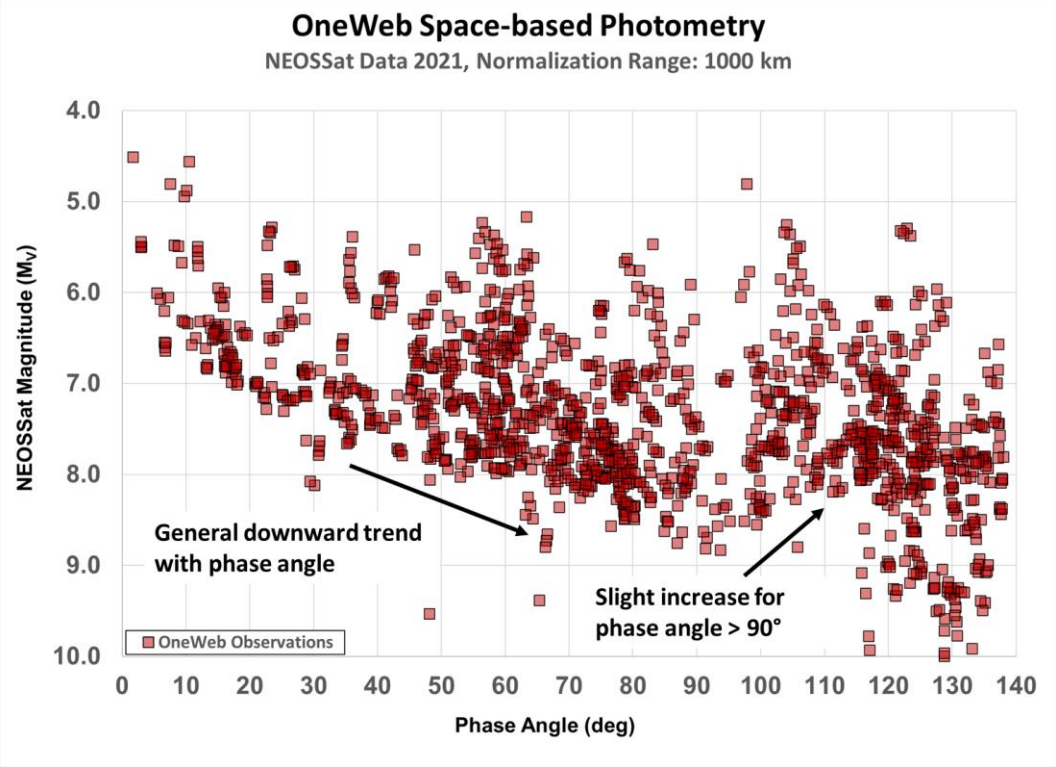

Fig. 18: Range normalized space-based photometry of the OneWeb constellation vs phase angle

OneWeb satellites orbit above NEOSSat thus the relative elevations of each OneWeb track ranged from -15° up to 30° above NEOSSat's local horizontal plane. Different portions of the OneWeb bus become visible to NEOSSat where NEOSSat can see the nadir face or angled keep-alive solar panels affixed to the main bus. The OneWeb Arrow satellite bus has a more complex prismatic shape compared to the Starlink satellite making attempts to determine the key

factors driving its photometry more complicated. The OneWeb attitude control profile is not known however it is likely to have a nadir-aligned, Sun-constrained orientation which orients its antennas earthward and the solar panels toward the Sun. Future analysis of OneWeb photometric data will examine if this attitude profile is consistent with the observed photometry.

8. FLOCK CHARACTERIZATION / RESULTS

Observations of the Planet Labs Flock constellation proved much more challenging than Starlink and OneWeb. Initial efforts to track Flock satellites began in June 2021 and yielded 31 observations of 9 unique Flock satellites. While Flock nanosatellites orbit at altitudes similar, or slightly lower than Starlink, the Flock nanosatellites have a vastly smaller bus size and generally resulted in fainter photometry (see Fig. 19) making them more challenging to obtain measurements. The apparent magnitudes, prior to range normalization, spanned M_v 7.6-13.3 and their range normalized magnitudes spanned M_v 5.9-11.2 with average M_v 9.4 ± 1.1. The ranges at detection spanned 1700-2800 km comparable to the Starlink observations.

To collect well-sampled background stars for future astrometric processing, the NEOSSat detector integration time was set to 1 second exposures. This inherently limits NEOSSat's sensitivity to M_v 13.5 objects which is consistent with NEOSSat's faintest detections made on the Flock satellites when imaging in 2x2 binned mode. This is a general challenge for space-based tracking of small objects in LEO from a LEO observation perspective where small objects require longer exposures to detect them, whereas the background stars are best imaged using shorter exposure lengths to form suitable in-frame star solutions for metric processing.

NEOSSat's observations on Flock were limited to lower phase angles where the nanosatellites are more directly sun-lit. Fig. 19 does show evidence where possible glinting behaviour is observed. The fainter target, combined with enhanced Earth glow from the lower altitude (see examples in Fig. 7) generally resulted in fewer successful observations on the Flock nanosatellites. Interestingly, three measurements from the smaller Flock nanosatellites did saturate NEOSSat's detector during observations. Unfortunately, not enough data was collected on the Flock satellites to fully characterize their behaviour over a larger swath of phase angles.

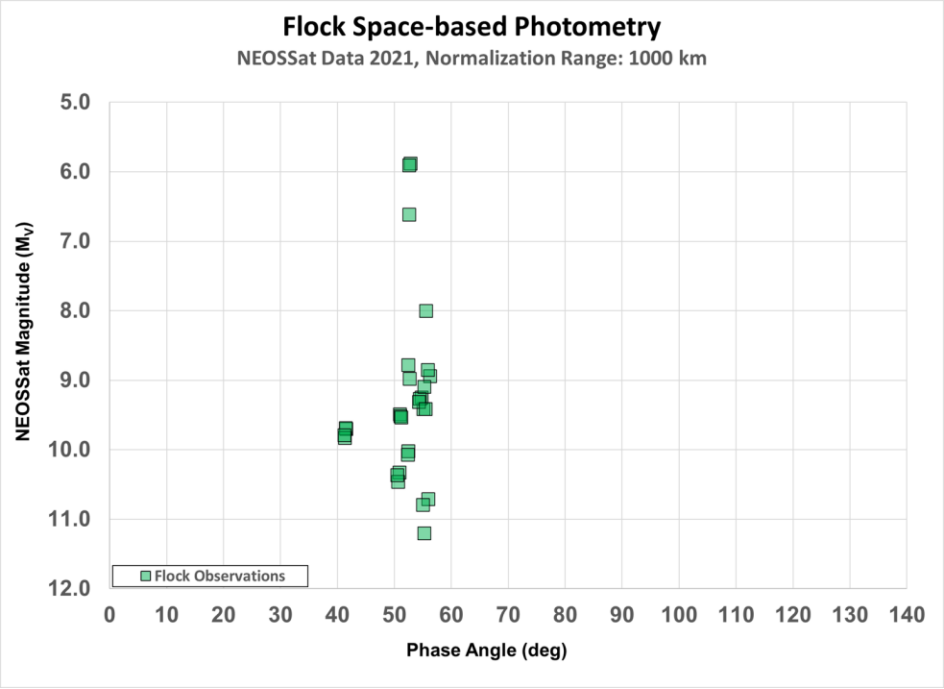

Fig. 19: Range normalized photometry of the Flock constellation vs phase angle

9. CONSTELLATION COMPARISON

Fig. 20 summarizes all space-based range-normalized photometric measurements in one comparison plot for Starlink, OneWeb and Flock satellites. In general, a discernible trend is observed over phase angle for the Starlink satellites, whereas the brightness trends in OneWeb is somewhat more difficult to discern due to their higher variability even at low phase angles. OneWeb photometry shows a weaker dependence on phase angle compared to the Starlink satellites when viewed from orbit. The Flock nanosatellites, with their inherent observing challenges, were primarily sampled over 22°-56° phase angle and did not provide enough diversity of observing geometry to fully compare to Starlink and OneWeb. Flock does show that it is inherently fainter than the larger broadband constellations, but more observing diversity is required to more properly describe their brightness behaviour when observed from space. It is notable that a Flock nanosatellite can be comparably as bright as Starlink and OneWeb satellites and is likely due to specular reflection from the surfaces of the vehicle.

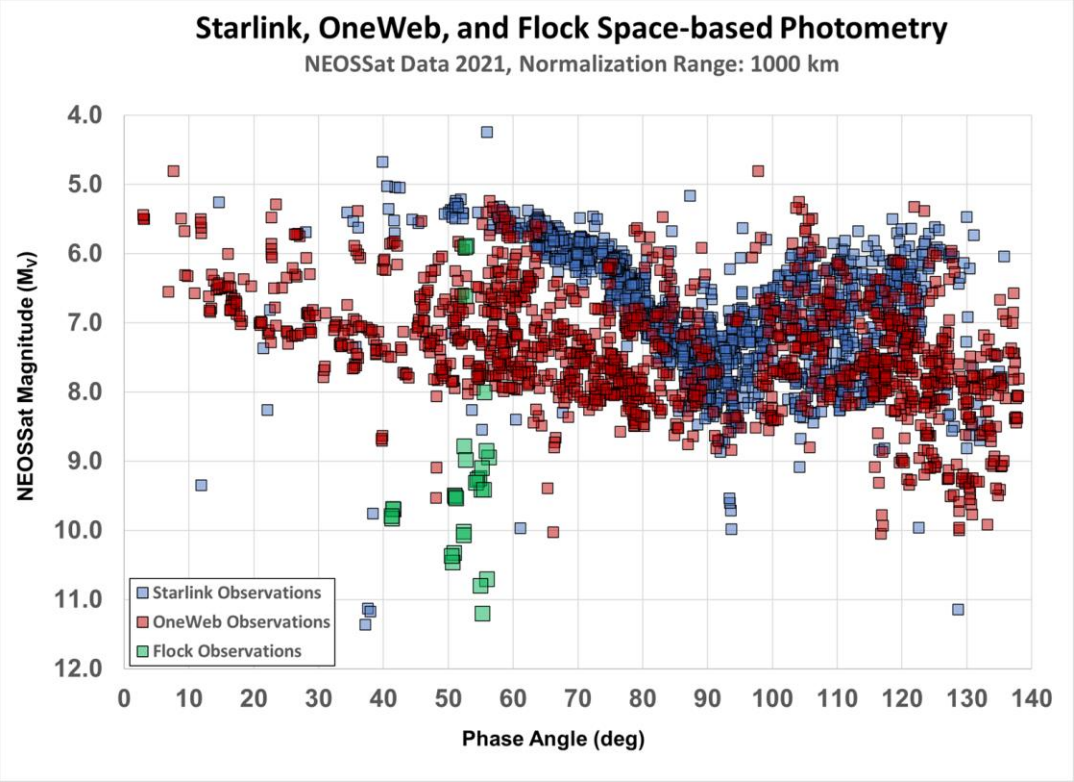

Fig. 20: Range normalized photometry of the Starlink, OneWeb and Flock constellations vs phase angle

10. CONCLUSION

NEOSSat collected space-based observations of the Starlink (2170 observations), OneWeb (1400 observations), and Flock (31 observations) constellations from orbit. NEOSSat's LEO nodal encounter approach was used to acquire photometric measurements producing tracklets which aggregated individual object tracklets together with other individual constellation members to produce light curves. This measurement set provides a first look at mega-constellation member brightness from orbit to help establish baseline geometric and visual characteristics of mega-constellation photometry when viewed from LEO. These measurements also compliment ground-based observers examining mega-constellations by sampling lower phase angles which can be challenging to observe by ground-based systems.

The Starlink constellation's relatively simple geometry and mass-produced number enabled baseline comparisons to be made against other constellations. Starlink was used as a LEO constellation mega-constellation photometric reference to compare others. The average space-based magnitude of 2170 photometric measurements of 412 unique Starlink satellites, including those equipped with a sun-reflecting visor, normalized to a range of 1000 km was found

to be M_v 6.9 ± 0.9 over a variety of space-based observing geometries. A notable fraction of the population showed detector saturation and their measurements were not included in the analysis of this dataset. When the Starlink satellites are over the dark limb of the Earth, a simple flat-plate model for the main solar array can be used in predicting a satellite's brightness based on the assumption that the solar panels are sun-pointing. The close adherence of the developed anti-solar model with the detected Starlink photometry suggests that the solar panels are primarily sun-pointing during their operation. A first order photometric model of dayside illumination (high phase angle) of the Starlink solar panel's backside suggests it is more reflective in comparison to its Sun-pointing side. The albedo-area products of the solar panel's backside and sun-facing side were found to be 10.5 m^2 and 0.9 m^2 respectively.

The OneWeb constellation was also assessed in this study. The average magnitude of 1400 photometric measurements of 81 unique OneWeb satellites, normalized for the standard satellite range of 1000 km, was found to be M_v 7.4 ± 0.8 over a variety of space-based observing geometries. After aggregating NEOSSat's tracklets no clear trend over phase angle is observable in OneWeb photometry as seen in the Starlink constellation however a weak dimming of brightness with phase angle was observed for phase angles from 0-90°. Some possible evidence of dayside brightening is shown, however the scatter in the OneWeb photometry cannot conclusively determine if this is the case. The more complex shape of the OneWeb satellites is attributed to be the cause of the variable photometry in addition to the wide variety of low and high elevation observing geometries possible from NEOSSat which presents various OneWeb satellite facets toward the observer. It is recommended that continued analysis of this data incorporate basic attitude profiles and shape models for the OneWeb satellites to attempt to better correlate measured photometry with their estimated shape and surface reflectivity.

Planet Labs Flock nanosatellites were examined also, but with fewer measurements. The average magnitude of 32 photometric measurements of 9 unique Flock satellites (also known as "Doves"), normalized for the standard satellite range of 1000 km, was found to be M_v 9.4 ± 1.1 over a limited range of space-based observing geometries. These smaller nanosatellites posed more of an observing challenge for NEOSSat due to their faintness and closer proximity to illuminated portions of the Earth limb. It is recommended to attempt continued measurements on the nanosatellite class but increase NEOSSat's imager exposure times at the expense of collecting well-sampled background star streaks. This will increase the likelihood of Flock nanosatellite detection for photometric measurement at the expense of lowered astrometric measurement quality.

This study revealed photometric contrasts between different mega-constellation satellite designs and revealed some complexities involved in tracking large LEO constellations from orbit. A strategy for LEO-to-LEO observation relative to the bright Earth limb and planning satellite SSA observations using TLE orbital data was obtained. This exploration helps increase understanding of new mega-constellation infrastructures in orbit and help build toward new observing modalities from LEO.

11. REFERENCES

[1] CelesTrack, "Satellite Catalog (SATCAT)," https://celestrak.com/satcat/search.php

[2] Johnson, C., Scott, R.L., Thorsteinson, S., "Space-based Photometric Observations of the SpaceX Starlink Constellation Satellites – Preliminary Findings", Canadian Aeronautics and Space Institute Astro Conference 2020, Ontario, Canada, (2020).

[3] Cognion, R.L, "Observations and Modelling of GEO Satellites at Large Phase Angles", AMOS Conference 2013, Poster Paper, Maui Economic Development Board (2013), https://amostech.com/TechnicalPapers/2013/POSTER/COGNION.pdf, accessed 8 Oct 2020.

[4] Space Exploration Holdings, LLC, Request for Modification of the Authorization for the SpaceX NGSO Satellite System, IBFS File No. SAT−MOD−20181108−00083, filed November 8, 2019.

[5] WorldVu Satellites Limited, OneWeb Ka-band NGSO constellation, FCC file No. SATLOI-20160428-00041, filed September 12, 2018.

[6] Bronson, Po. "A Dove's Eye View." Alta Online, 29 Nov. 2020, www.altaonline.com/dispatches/a4923/a-doves-eye-view/.

[7] Scott, R.L., Thorsteinson, S., "Key Findings from the NEOSSat Space-Based SSA Microsatellite Mission", AMOS Technical Conference 2018, Maui, HI, (2018).

[8] Arlo U. Landolt, "UBVRI Photometric Standard Stars Around the Celestial Equator: Updates and Additions," Astron. J. 137, 4186 (2009)

[9] CelesTrak, “Current Supplemental Two-Line Element Sets,” https://celestrak.com/NORAD/elements/supplemental/
[10] Hainaut, Olivier R., and Andrew P. Williams. “Impact of Satellite Constellations on Astronomical Observations with ESO Telescopes in the Visible and Infrared Domains.” Astronomy & Astrophysics, vol. 636, 2020, doi:10.1051/0004-6361/202037501.
[11] Mallama, Anthony. “Starlink Satellite Brightness Before Visorsat.” ArXiv.org, 15 June 2020, https://arxiv.org/ftp/arxiv/papers/2006/2006.08422.pdf.
[12] Mallama, Anthony. “The Brightness of OneWeb Satellites.” ArXiv.org, 9 Dec. 2020, https://arxiv.org/ftp/arxiv/papers/2012/2012.05100.pdf
[13] Mallama, Anthony. “The Brightness of VisorSat-Design Starlink Satellites.” ArXiv.org, 2 Jan. 2021, https://arxiv.org/ftp/arxiv/papers/2101/2101.00374.pdf